

Predicting Networks Before They Happen: Experimentation on a Real-Time V2X Digital Twin

Roberto Pegurri¹, Shintaro Habu², Francesco Linsalata¹, Kui Wang², Tao Yu²,
Eugenio Moro¹, Maiya Igarashi², Antonio Capone¹, Kei Sakaguchi²

¹*Department of Electronics, Information and Bioengineering, Politecnico di Milano, Italy*

²*Department of Electrical and Electronic Engineering, Institute of Science Tokyo, Japan*

Email: ¹{name.surname}@polimi.it, ²{habu, kuiw, yutao, igarashi, sakaguchi}@mobile.ee.titech.ac.jp

Abstract—Emerging safety-critical Vehicle-to-Everything (V2X) applications require networks to proactively adapt to rapid environmental changes rather than merely reacting to them. While Network Digital Twins (NDTs) offer a pathway to such predictive capabilities, existing solutions typically struggle to reconcile high-fidelity physical modeling with strict real-time constraints. This paper presents a novel, end-to-end real-time V2X Digital Twin framework that integrates live mobility tracking with deterministic channel simulation. By coupling the Tokyo Mobility Digital Twin—which provides live sensing and trajectory forecasting—with VaN3Twin—a full-stack simulator with ray tracing—we enable the prediction of network performance before physical events occur. We validate this approach through an experimental proof-of-concept deployed in Tokyo, Japan, featuring connected vehicles operating on 60 GHz links. Our results demonstrate the system’s ability to predict Received Signal Strength (RSSI) with a maximum average error of 1.01 dB and reliably forecast Line-of-Sight (LoS) transitions within a maximum average end-to-end system latency of 250 ms, depending on the ray tracing level of detail. Furthermore, we quantify the fundamental trade-offs between digital model fidelity, computational latency, and trajectory prediction horizons, proving that high-fidelity and predictive digital twins are feasible in real-world urban environments.

Index Terms—NDT, V2X, Real-Time, Ray Tracing

I. INTRODUCTION

Connected and automated vehicles are pushing wireless networks to operate increasingly close to their physical limits, both in terms of reliability and reaction time. Safety critical Vehicle-to-Everything (V2X) applications such as collision avoidance, cooperative perception, and automated intersection management require the network to reason not only about the current state of the environment, but also on how positions and channels will evolve in the immediate future, from tens of milliseconds to a few seconds ahead [1]. This is precisely the promise of Network Digital Twins (NDTs): a software replica of the physical system, continuously synchronized with live data, that can be queried to evaluate “what-if” situations before they affect real users [2]. Despite significant progress, most existing NDTs operate in an essentially *offline* manner. High-fidelity ray tracing, realistic mobility engines, and multi-RAT protocol stacks are routinely used to obtain accurate performance evaluations, but without strict timing constraints, simulation runs may take seconds, minutes, or even hours to complete. This is acceptable for design-time analysis, but incompatible with an online, predictive Digital Twin (DT),

for which results must be delivered within the tight latency budget [3], for example as imposed by V2X applications. If the twin delivers its prediction too late, vehicles will have moved, the channel will have changed, and any recommended action may already be obsolete or even unsafe. Two recent platforms partially address this gap. The *Tokyo Mobility DT*—from here on referred to as *Mobility DT*—developed by the Institute of Science Tokyo, Japan [4] provides a detailed 3D reconstruction of the Ookayama Campus area in Tokyo, Japan. It supports both real-time and replayed trajectories enabling realistic urban-scale mobility scenarios. Conversely, *VaN3Twin* [5] extends the *ms-van3t/ns-3* framework [6] with the in-the-loop integration of Sionna RT [7], thereby enabling deterministic ray-based channel prediction and the implementation of Intelligent Transportation Systems (ITS) protocols over full-stack realizations of multiple Radio Access Technologies (RATs). The resulting framework has been validated against on-field measurements, demonstrating close agreement between predicted and observed channel behavior [5].

Each platform solves a different part of the problem: the *Mobility DT* offers realism in geometry and mobility, while *VaN3Twin* offers realism across the complete communication stack. Neither, however, provides an end-to-end real-time pipeline capable of ingesting live mobility, predicting near-future trajectories, computing near-future channels, and take action within a strict deadline.

A. State of the art

General-purpose network simulators such as *ns-3* and *OM-NeT++* form the foundation of most V2X simulation frameworks. Among them, *ms-van3t* is one of the most comprehensive: it supports IEEE 802.11p, LTE-V2X, NR-V2X, and the full ETSI ITS-G5 facilities layer, and integrates with SUMO and CARLA for mobility simulation [6]. Several recent works interpret such simulators as components of broader vehicular NDTs. Examples include blockage-aware mmWave DTs for multi-hop topologies [8] and multi-modal DTs combining mobility, sensing, and coarse communication abstractions [9]. These platforms move beyond offline simulation but still rely on simplified PHY abstractions to maintain responsiveness. Traditional wireless propagation models in *ns-3* and *OM-NeT++* are stochastic (e.g., 3GPP TR 36.885/38.901) or based on analytical families such as WINNER, able to capture

large-scale trends but not the site-specific multipath structure. This limitation becomes critical in DT settings, where small changes in geometry or mobility strongly influence short-term channel evolution. To overcome this, several works integrate external ray-based channel simulators into network simulators. MATLAB-based approaches [10] emphasize PHY accuracy and hardware emulation, but lack full V2X stacks and exhibit poor scalability. Other works import offline ray-traced maps into ns-3 [11], enabling bit-level simulation but preventing synchronous updates. OPAL-OMNeT++ integration [12] achieves realistic geometry but targets non-V2X technologies. VaN3Twin, however, advances this direction by coupling ms-van3t with Sionna RT into a comprehensive V2X NDT framework, enabling high-fidelity, in-the-loop ray-traced propagation and realistic modeling of multi-RAT co-existence over shared spectrum portions. However, despite its channel realism, VaN3Twin has primarily been used offline or in emulation mode, without enforcing a strict real-time prediction deadline. GPU-accelerated ray tracing software such as Sionna RT now enable repeated evaluations with competitive runtime [13]. This has motivated new in-the-loop architectures, including ns3sionna [14] for Wi-Fi and our prior ns-3 + Sionna RT integration [15] for multi-RAT 6G studies. DT-CoVeSS [16] similarly uses Sionna RT for high-fidelity analysis of CV2X security. These works demonstrate that in-the-loop ray tracing integration is feasible, but none targets city-scale mobility, full V2X communication stacks, and strict prediction deadlines simultaneously. Vehicular DTs outside ns-3 focus increasingly on near real-time operation. RAVEN [17] combines live data and contextual information to predict mmWave conditions and support interference management. Vehicle-to-Cloud ADAS [18] demonstrates cloud-assisted actuation using DT logic. Large-scale mobility DTs such as TuST [19] and indoor crowd models [20] show that realistic spatio-temporal digital replicas can be built from real data. However, these systems often rely on simplified communication models or separate mobility and communication loops. What is missing is a DT that combines: (i) realistic, city-scale mobility; (ii) a full-stack, ray-traced V2X simulator; and (iii) an explicit timing budget ensuring that predictions are delivered before the event takes place in the physical world.

Paper Contributions To address the gap identified above, we integrate VaN3Twin within the Tokyo Mobility DT ecosystem using Sionna RT as a shared ray tracing core, orchestrating data exchange and scheduling to enable short-term *future* channel prediction at latencies compatible with real-time V2X operation. Any predictions that arrive too late are discarded to maintain consistency with the evolving physical system. This integration exposes the key challenges of real-time NDT operation, including the computational cost of ray-traced propagation, the synchronization of mobility and geometry between platforms, and the scheduling required to deliver actionable predictions before the corresponding physical time occurs. Rather than proposing new trajectory or channel prediction algorithms, our goal is to quantify how far a real system can be pushed toward real-time predictive operation when combining

a live mobility testbed with a high-fidelity V2X DT.

The main contributions of this work are as follows:

- We design and implement an end-to-end integration of VaN3Twin and the Tokyo Mobility DT into a latency-aware and predictive NDT;
- We introduce a timing-constrained workflow for future channel state prediction, where mobility updates, 3D scene synchronization, ray tracing, and network simulation are orchestrated to meet a strict latency budget;
- We demonstrate the integrated system in an urban testbed, quantifying the trade-offs between trajectory prediction error, channel prediction accuracy, and system latency.

Paper Organization The remainder of the paper is structured as follows. Section II presents the integration architecture and the real-time workflow. Section III formalizes how model complexity affects computation time and end-to-end system latency. Section IV reports experimental results from the physical deployment in the Ookayama Campus of the Institute of Science Tokyo, Japan. Section V concludes the paper.

II. INTEGRATION ARCHITECTURE

This section presents the architecture of the proposed framework and details the interactions among its main components. As shown in Figure 1, the framework integrates three core components: (i) The *physical entities*, i.e., the vehicles equipped with sensing and communication capabilities; (ii) The *Mobility DT*, which maintains a live digital replica of the surrounding traffic and predicts short-term future mobility states; (iii) *VaN3Twin*, the NDT engine responsible for full-stack replication and prediction of V2X communication processes. Physical entities provide time-stamped measurements to the Mobility DT, which produces short-term mobility predictions for VaN3Twin. VaN3Twin uses these predictions to simulate future communication states and returns per-link KPIs. In this architecture, the Mobility DT serves as the coordinating component of the system. It aggregates real-time mobility and perception data collected by LiDAR-equipped physical entities as well as by LiDAR and camera sensors mounted on nearby Road Side Units (RSUs) or, eventually,

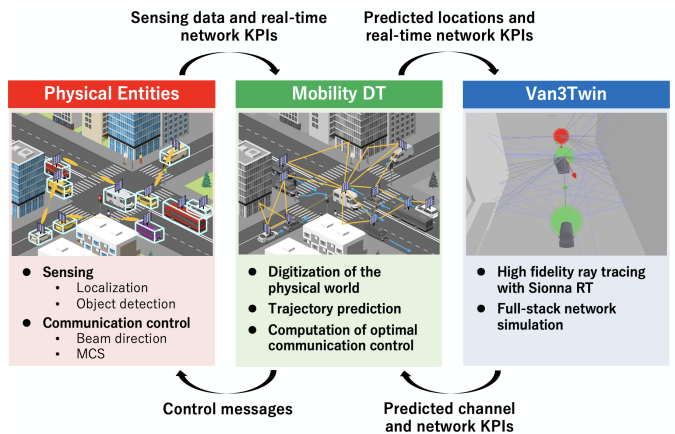


Fig. 1: Schematic architecture of the framework.

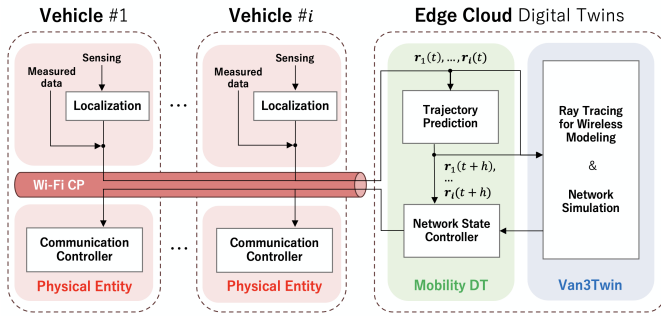


Fig. 2: End-to-end communication workflow.

network-enabled positioning techniques [21]. Using this information, it continuously maintains and forecasts the mobility state of all dynamic elements in the scenario. Mobility updates are processed at a fixed, pre-defined rate, and predictions are generated for a single, short-term horizon h , selected to remain compatible with the end-to-end latency budget of the system. The prediction horizon is kept fixed during operation to ensure deterministic scheduling and bounded computation time. The Mobility DT then orchestrates network-level prediction requests to VaN3Twin and subsequently disseminates predicted communication states back to the physical entities—possibly including control commands to be applied to the network configuration. Communication between system elements is structured according to their functional roles. A specific physical entity provides the interface between physical entities and the Mobility DT, leveraging a 2.4 GHz IEEE 802.11n Wi-Fi Control Plane (CP) for low-latency over-the-air control operations. Meanwhile, the Mobility DT and VaN3Twin communicate over a wired Ethernet Local Area Network (LAN), reflecting their co-location at the network edge to minimize latency. All inter-component exchanges employ lightweight UDP messages with JSON-formatted payloads, enabling efficient and low-overhead transmission of state and control information. Message delivery is best-effort: occasional packet losses are tolerated and naturally compensated for by subsequent updates, avoiding retransmission delays. All components rely on a shared time base, with timestamps carried in each message and clocks synchronized using standard network time synchronization mechanisms, ensuring consistent temporal alignment across mobility and communication predictions. The detailed data exchange loop is described in the following subsection.

A. End-to-end Workflow

The end-to-end workflow illustrated in Figure 2 specifies all the interactions introduced above and clarifies how mobility prediction and communication prediction are coupled in practice. Physical entities periodically transmit their sensed location and measured communication data to the Mobility DT—located in the edge cloud—with an implementation-dependent reporting period Δt_{PE} . These updates are timestamped and provide the input required to keep the digital

replica synchronized with the physical system and to continuously adjust the internal prediction models. Based on the aggregated and synchronized mobility state, the Mobility DT computes short-term trajectory forecasts for all relevant dynamic objects. Network prediction requests to VaN3Twin are then generated according to a configurable policy, which may be periodic or event-driven, and always target a single future time instant $t + h$. The prediction horizon h is chosen so as to remain compatible with the end-to-end latency budget; multi-horizon requests are also possible in principle but are outside the scope of this work. Upon receiving a request, VaN3Twin generates a future communication scenario corresponding to the target time $t + h$. Predicted vehicle poses are used to construct a consistent 3D scene, which serves as input to the deterministic ray-based channel model formalized in Section III. The resulting channel realizations drive full-stack V2X simulations, possibly yielding protocol- and packet-level performance indicators. In parallel, the recently observed communication measurements are used to compensate for systematic prediction biases, such as offsets in the computed received power. The predicted communication state is then returned to the Mobility DT and made available for network-level decision making. When required, the DT translates these predictions into control actions which are conveyed back to the physical entities over the dedicated Wi-Fi CP, thereby closing the loop between the digital and physical domains. To reason about the limits of this approach, the next section provides a formal characterization of the proposed integration, detailing the underlying trajectory prediction model, the channel estimation process, and the resulting trade-offs between model complexity, end-to-end latency, and the maximum achievable prediction horizon.

III. END-TO-END ANALYSIS

This section provides a formal characterization of the integration presented in Section II. We describe the trajectory prediction model, formalize the ray-based channel prediction process, and introduce a concise characterization of model complexity that links physical-model fidelity to end-to-end latency and feasible prediction horizons.

A. Mobility and Channel Prediction

Each vehicle i in the scenario is represented by the kinematic state $\mathbf{x}_t^i = (\mathbf{p}_t^i, \mathbf{v}_t^i, \psi_t^i)$. The state evolution assumes a constant-velocity motion model, with \mathbf{F}_t^i defined accordingly based on the sampling interval. \mathbf{z}_t^i represents the state measurement vector, which the DT fuses into a unified state estimate. The temporal evolution of each vehicle follows a linear state-space model defined by the state-transition matrix \mathbf{F}_t^i , the control-input matrix \mathbf{B}_t^i , and the measurement model matrix \mathbf{M}_t^i , with process noise covariance \mathbf{Q}_t^i and measurement noise covariance \mathbf{R}_t^i . The process noise covariance \mathbf{Q}_t^i accounts for deviations from ideal constant-velocity motion and is treated as a design parameter, whereas the measurement noise covariance \mathbf{R}_t^i is sensor-dependent and reflects the heterogeneous accuracy of the contributing sensing modalities. Given the

Algorithm 1 Trajectory Prediction for Vehicle i

Require: $\hat{\mathbf{x}}_{t-1|t-1}^i, \mathbf{P}_{t-1|t-1}^i, \mathbf{z}_t^i, h$

- 1: Prediction:
 - 2: $\hat{\mathbf{x}}_{t|t-1}^i = \mathbf{F}_t^i \hat{\mathbf{x}}_{t-1|t-1}^i + \mathbf{B}_t^i \mathbf{u}_t^i$
 - 3: $\mathbf{P}_{t|t-1}^i = \mathbf{F}_t^i \mathbf{P}_{t-1|t-1}^i (\mathbf{F}_t^i)^\top + \mathbf{Q}_t^i$
 - 4: Update:
 - 5: $\mathbf{K}_t^i = \mathbf{P}_{t|t-1}^i (\mathbf{M}_t^i)^\top (\mathbf{M}_t^i \mathbf{P}_{t|t-1}^i (\mathbf{M}_t^i)^\top + \mathbf{R}_t^i)^{-1}$
 - 6: $\hat{\mathbf{x}}_{t|t}^i = \hat{\mathbf{x}}_{t|t-1}^i + \mathbf{K}_t^i (\mathbf{z}_t^i - \mathbf{M}_t^i \hat{\mathbf{x}}_{t|t-1}^i)$
 - 7: $\mathbf{P}_{t|t}^i = (\mathbf{I} - \mathbf{K}_t^i \mathbf{M}_t^i) \mathbf{P}_{t|t-1}^i$
 - 8: Horizon propagation:
 - 9: $\hat{\mathbf{x}}_{t+h|t}^i = (\mathbf{F}_t^i)^h \hat{\mathbf{x}}_{t|t}^i$
 - 10: **Return:** predicted pose $\hat{\mathbf{x}}_{t+h|t}^i$
-

filtered estimate at time t , the DT propagates the state h steps forward to obtain the predicted pose $\hat{\mathbf{x}}_{t+h|t}^i$, which defines the forecasted traffic geometry used for channel prediction (Algorithm 1). Once the future scene configuration is assembled, the DT evaluates the wireless channel through a deterministic ray-based propagation model. For each transmitter–receiver pair (i, j) , the ray tracing engine emits N_{rays} rays from the antenna of vehicle i , with departure directions covering the unit sphere. Each ray propagates through the environment and may undergo up to N_{int} interactions with surrounding surfaces. A ray reaching the antenna of vehicle j is part of a valid propagation path that is added to the set $\mathcal{P}_{\text{valid}}^{i,j}$. Each path $p \in \mathcal{P}_{\text{valid}}^{i,j}$ is characterized by its length $d_p^{i,j}$, delay $\tau_p^{i,j} = d_p^{i,j}/c$, angles of departure $(\theta_{\text{T}}^{(p)}, \varphi_{\text{T}}^{(p)})$ and arrival $(\theta_{\text{R}}^{(p)}, \varphi_{\text{R}}^{(p)})$, and by an ordered sequence of N_p interactions. Its effect on the received field is described by the 2×2 propagation matrix:

$$\mathbf{A}_p^{i,j} = \left(\frac{\lambda}{4\pi d_p^{i,j}} \right) e^{-j \frac{2\pi}{\lambda} d_p^{i,j}} \prod_{\ell=1}^{N_p} \mathbf{M}_p^{(\ell)}, \quad (1)$$

where each $\mathbf{M}_p^{(\ell)}$ models the polarization-dependent transformation induced by the ℓ -th interaction. The transmit and receive antennas are represented through their complex pattern vectors $\mathbf{c}_{\text{T}}(\theta, \varphi)$ and $\mathbf{c}_{\text{R}}(\theta, \varphi)$. The scalar baseband contribution of path p to the channel between vehicles i and j is then

$$g_p^{i,j} = \mathbf{c}_{\text{R}}^H(\theta_{\text{R}}^{(p)}, \varphi_{\text{R}}^{(p)}) \mathbf{A}_p^{i,j} \mathbf{c}_{\text{T}}(\theta_{\text{T}}^{(p)}, \varphi_{\text{T}}^{(p)}). \quad (2)$$

The predicted multipath channel at time $t+h$ is therefore

$$h_{t+h|t}^{i,j}(\tau) = \sum_{p \in \mathcal{P}_{\text{valid}}^{i,j}} g_p^{i,j} \delta(\tau - \tau_p^{i,j}). \quad (3)$$

Collecting all pairwise impulse responses yields the predicted channel matrix $\hat{\mathbf{H}}_{t+h|t} = (h_{t+h|t}^{i,j})_{i,j \in \mathcal{V}}$.

B. Computational Complexity and Execution Time

Let τ_{e2e} be the total time elapsed between the acquisition of a measurement by a vehicle and the completion of the corresponding DT update. Formally:

$$\tau_{e2e} = \tau_m + \tau_w + \tau_{tp} + \tau_{req} + \tau_{rt} + \tau_{req} + \tau_w, \quad (4)$$

TABLE I: Ray tracing parameters for each Density Index (DI).

RT Parameter	DI 1	DI 2	DI 3	DI 4	DI 5
# Max. Interactions	3	3	5	8	8
# Rays per source	10^3	10^3	10^6	10^{10}	10^{10}
Direct LoS Path	✓	✓	✓	✓	✓
Specular reflection	×	✓	✓	✓	✓
Diffuse reflection	×	×	✓	✓	✓
Refraction	×	×	×	✓	✓
Diffraction	×	×	×	×	✓

where τ_m is the measurement acquisition time, τ_w the communication delay between vehicles and the Mobility DT, τ_{tp} the Mobility DT update and trajectory prediction time, τ_{req} the inter-process communication delay, and τ_{rt} the execution time of the physical-modeling stage. Given the computational complexity of the ray tracing operation, τ_{rt} is the dominant and most variable component. Specifically, it depends on the level of physical detail included in the propagation model. To describe these configurations in a compact and general manner, we introduce the *Ray Tracing Detail Index*, denoted DI, a scalar metric used to classify the fidelity level of the physical-modeling stage. Each DI level corresponds to a specific configuration of the physical model, ranging from lightweight approximations to high-fidelity representations. Table I reports the five DI levels considered in this work. Lower levels include only the essential components needed for coarse propagation estimates, whereas higher levels progressively incorporate more detailed interaction mechanisms, finer spatial resolution, and higher-order multipath modeling. Although in our implementation these fidelity levels map to different configurations of a ray-based propagation model, the abstraction provided by DI remains general and applicable to any physical-modeling backend that supports multiple complexity tiers. As the DI increases, the execution time of the physical model, denoted τ_{rt} , grows accordingly.

To ensure causality, the prediction horizon h must exceed the end-to-end latency τ_{e2e} . Increasing model fidelity therefore requires larger horizons, which in turn amplify trajectory prediction errors and their impact on channel estimation, revealing a fundamental trade-off between physical-model complexity, latency, and predictive accuracy. Section IV provides an empirical characterization of these trade-offs based on real-world experiments conducted in Tokyo, Japan, evaluating how different DI levels impact both computational latency and channel prediction accuracy.

IV. EXPERIMENTAL AND SIMULATED RESULTS

To demonstrate the practical operation of the proposed system, we consider a proof-of-concept deployment carried out in the Ookayama campus of the Institute of Science Tokyo, Japan including measured end-to-end latencies. To complement the experimental analysis, we then consider a simulation study performed in the identical geometric scenario in which we systematically vary the DI and introduce synthetic perturbations into the trajectory prediction module.

TABLE II: VaN3Twin settings for ray tracing.

RT Settings	Value
Carrier Frequency	60 GHz
Buildings and Roads Material	Concrete [22]
Trees Material	Wood [22]
Cars Material	Metal [22]
Type of Antennas	Panasonic WiGig RSU
Polarization	Vertical
Digital Model DI	DI 5 (see Tab. I)

A. Scenario introduction

The evaluation scenario involves three connected vehicles (Figure 3a) that interact with the Mobility DT through a 2.4 GHz Wi-Fi CP, and are each equipped with a roof-mounted Panasonic WiGig RSU forming the 60 GHz high-capacity User Plane (UP). The Mobility DT and VaN3Twin are deployed at the edge—corresponding to the location of Vehicle 3—and exchange data through a wired Ethernet LAN. Figure 3b illustrates the corresponding VaN3Twin ray tracing scenario of the considered street in Ookayama, Tokyo, Japan. Buildings, vehicles, and antennas are modeled in VaN3Twin using material properties and radiation patterns consistent with the experimental setup (see Table II). VaN3Twin ray tracing details are reported in Table II. During the experimental campaign, the vehicles perform `iperf`-based data transmissions over the WiGig UP. Vehicle 1 (a Toyota COMS) and Vehicle 3 (a motorized wheel cart) remain stationary and maintain a direct Line of Sight (LoS) link, while Vehicle 2 (a Toyota Estima) follows a predefined trajectory (Figure 3b) that intermittently blocks the LoS path. The Mobility DT is used to predict, in real time, the 60 GHz channel between Vehicles 1 and 3 via VaN3Twin, based on the predicted trajectory of Vehicle 2 with prediction horizon $h = 500$ ms. Such predictions may be employed, for example, for proactive network topology management. The Mobility DT simultaneously collects from each vehicle its current position and the field-measured Received Signal Strength Indicators (RSSIs), which are employed for in-the-loop calibration of the prediction process. After computation, a control message is sent to the vehicles through the Wi-Fi CP. To quantify the effectiveness of this real-time predictive loop, we evaluate the accuracy of the RSSI forecasts produced by VaN3Twin along the trajectory of Vehicle 2. The Mobility DT employs the simple predictor for short-term trajectory estimation presented in Section III-A, while VaN3Twin operates using the DI 5 configuration reported in Table I. Results show a maximum average RSSI prediction error of 1.01 dB and a 95th-percentile error of 3.05 dB, demonstrating accurate prediction of the 60 GHz link dynamics under mobility-induced obstruction. Since VaN3Twin operates on predicted positions, channel accuracy is jointly limited by trajectory prediction error and by the selected ray tracing DI, which directly determines the end-to-end latency and thus the minimum prediction horizon required for real-time operation.

TABLE III: Fixed latency components contributing to τ_{e2e} .

Component	Resulting average
Measurement acquisition τ_m	8.9 ms
Wi-Fi CP communication τ_w	1.1 ms
Trajectory prediction τ_{tp}	4.4 ms
DT-VaN3Twin communication τ_{req}	0.6 ms
Total fixed latency	16.2 ms

B. End-to-End System Latency

Building on the formal definition introduced in Section III-B, this section reports on-field measurements of the end-to-end latency τ_{e2e} , decomposed according to (4).

Fixed system latency components: are summarized in Table III and constitute a fixed system latency budget, independent of the DI configuration. Measurement acquisition (τ_m) was evaluated by collecting location and channel samples over 60 s with a 100 ms sampling interval, yielding approximately 600 samples per experiment. No statistically significant differences were observed between static and dynamic conditions. Communication-related delays (τ_w and τ_{req}) were measured using ICMP-based Round Trip Time (RTT) probing over 100 messages and conservatively converted to one-way latency by halving the resulting value. Mobility DT update time and trajectory prediction latency (τ_{tp}) was obtained by profiling the time from the scenario update up to the execution of the linear prediction algorithm described in Section III-A.

Ray tracing execution times (τ_{rt}): were measured for the five DI configurations defined in Table I using VaN3Twin with Sionna RT v1.2.1. Experiments were conducted on a workstation with an NVIDIA GeForce RTX 3090 GPU and Intel Core i9-10980XE CPUs running Ubuntu 22.04.5. τ_{rt} increases monotonically with the DI level, reflecting the higher computational load induced by denser ray interactions and more complex propagation mechanisms.

End-to-end latency τ_{e2e} : is obtained by combining the fixed system latency components with the DI-dependent ray tracing execution time. The distributions of τ_{e2e} in Figure 4 show increasing latency and variability with ray tracing complexity, peaking at an average 250 ms for DI 5.

These results demonstrate that improving channel modeling fidelity by increasing the DI level inevitably enlarges the end-to-end latency budget. Since channel prediction must be available before transmission, this latency directly translates into a minimum required trajectory prediction horizon. As a result, higher-fidelity channel modeling forces the DT to rely on longer-term mobility forecasts.

C. Impact of trajectory prediction error

Because the end-to-end latency of the DT determines how far into the future vehicle positions must be predicted, longer latencies inevitably exacerbate trajectory prediction errors. This section quantifies how such latency-induced positional inaccuracies propagate into ray-traced channel prediction.

Let $\mathbf{p}(t) = [x(t), y(t)]^\top$ denote the ground-truth position at time t , and $\tilde{\mathbf{p}}(t) = \mathbf{p}(t) + \mathbf{e}(t)$ its perturbed counterpart, where

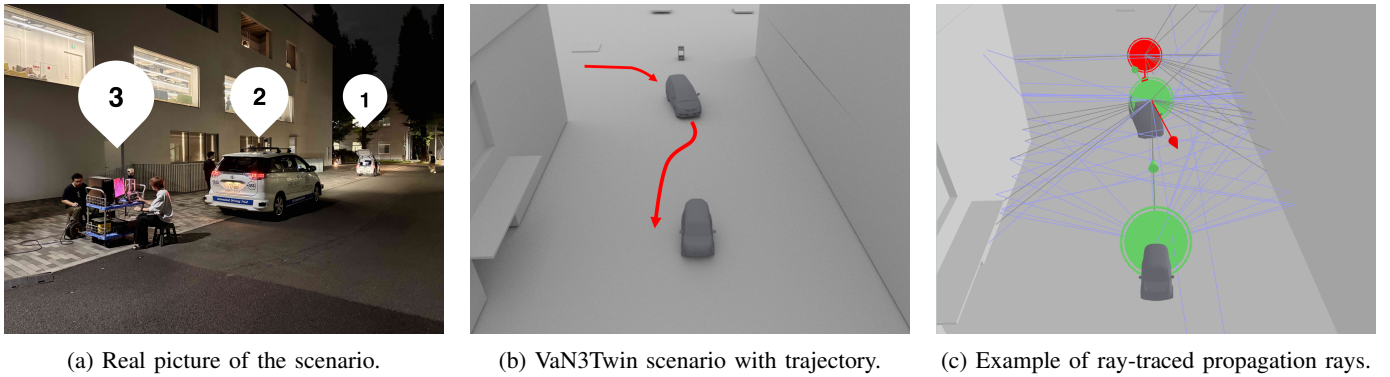


Fig. 3: Real picture (a), the corresponding VaN3Twin ray tracing representation (b), and an example of the computed propagation rays (c) of the road segment used in the experiments on the Ookayama campus of the Institute of Science Tokyo, Japan.

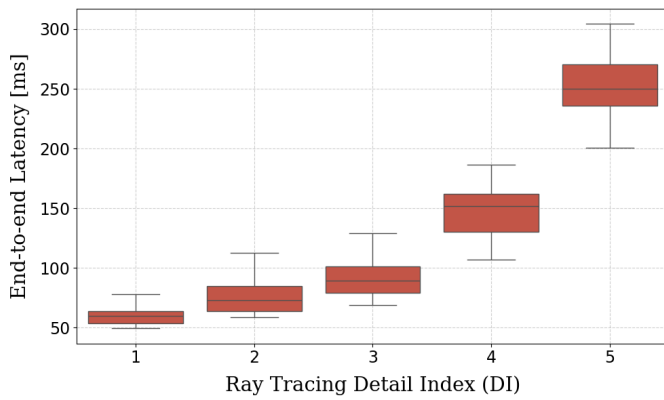


Fig. 4: Distribution of the measured end-to-end latency τ_{e2e} for different Ray Tracing DI configurations.

$\mathbf{e}(t)$ models the prediction error. A normalized parameter $k \in [0, 1]$ controls the maximum error magnitude through $\varepsilon_k = k \varepsilon_{\max}$, with $\varepsilon_{\max} = 1$ m in the considered setup. The displacement vector is sampled uniformly from a circular annulus $\mathbf{e}(t) \sim \mathcal{A}(\frac{1}{3}\varepsilon_k, \frac{1}{2}\varepsilon_k)$, and $\mathbf{e}(t)$ is isotropically sampled within the annulus itself. To quantify the impact of trajectory prediction inaccuracies, we evaluate two complementary metrics: (i) the deviation in received signal strength and (ii) the stability of the geometric visibility state. Both metrics are computed by comparing the channels obtained from the perturbed positions $\tilde{\mathbf{p}}(t)$ with those obtained from the true positions $\mathbf{p}(t)$.

RSSI Prediction Error: let $\text{RSSI}(t)$ denote the RSSI computed from $\mathbf{p}(t)$, and let $\widetilde{\text{RSSI}}(t)$ denote the value obtained from $\tilde{\mathbf{p}}(t)$. The discrepancy induced by a perturbation index k is measured through the Root Mean Squared Error (RMSE):

$$\text{RMSE}_k = \sqrt{\frac{1}{N} \sum_{t=1}^N \left(\widetilde{\text{RSSI}}(t) - \text{RSSI}(t) \right)^2}, \quad (5)$$

where N is the number of channel realizations. Figure 5 shows the dependence of the computed RMSE (blue) on the perturbation level k , focusing on measurements collected

during the LoS to non-LoS transition caused by the obstructing vehicle (Vehicle 2). The relationship is clearly non-linear, with a rapid increase in error for small positional deviations. For the considered scenario, $k \approx 0.1$ already yields an RMSE of approximately 20 dB in the RSSI prediction. Since small geometric inaccuracies already induce large prediction errors, these results also foreshadow the sensitivity of the LoS classification, analyzed next.

LoS Classification Robustness: trajectory perturbations may also change the geometric visibility between a transmitter and a receiver. Let $\text{LoS}_{\text{ref}}(t)$ denote the visibility classification obtained from $\mathbf{p}(t)$ and $\text{LoS}(t)$ that obtained from $\tilde{\mathbf{p}}(t)$. The robustness of the visibility classification under perturbation level k is expressed by

$$\eta_k = \frac{\text{TP}_k + \text{TN}_k}{N}, \quad (6)$$

where TP_k counts the instants for which both classifications report a LoS condition and TN_k counts the instants for which both report a non-LoS condition. The metric η_k therefore quantifies the agreement between the reference and perturbed LoS classifications under a positional perturbation of magnitude k . Figure 5 shows η_k (green) as a function of k . The geometric visibility prediction accuracy decreases monotonically, indicating a steady degradation of classification reliability with increasing positional error. For $k < 0.1$, the accuracy remains close to 100%, whereas it degrades substantially as k increases. At the maximum considered error, $\varepsilon_k \approx 1$ m ($k = 1$), the consistency drops to about 75%.

In conclusion, positional errors induced by longer prediction horizons offset the gains of high-fidelity ray tracing, exposing a fundamental trade-off between channel modeling precision and end-to-end latency.

V. CONCLUSIONS

In this work we presented and experimentally validated a real-time, predictive NDT for V2X communications, explicitly designed around end-to-end latency constraints. By integrating a live Mobility Digital Twin with the VaN3Twin engine, we implemented a closed-loop workflow capable of operating in

synchrony with the physical environment. A key outcome of this study is the end-to-end latency analysis of the Digital Twin pipeline, covering sensing, mobility prediction, ray-tracing-based channel computation, and data exchange. This analysis allowed us to identify how the computational complexity of the physical model directly constrains the feasible prediction horizon and, consequently, the usefulness of the Digital Twin for real-time operation. Experimental results obtained in a live urban environment demonstrate that high-fidelity channel modeling can be executed within a bounded time budget, provided that model complexity and scheduling are jointly designed. Overall, this work shows that real-time integration of mobility Digital Twins and ray-tracing-based network modeling is feasible and practically deployable. Future work will extend this latency-aware framework toward real-time prediction of higher-layer network performance metrics leveraging VaN3Twin full-stack V2X simulation capability.

ACKNOWLEDGMENT

This work was partially supported by the European Union - Next Generation EU under the Italian National Recovery and Resilience Plan (NRRP), Mission 4, Component 2, Investment 1.3, CUP D43C22003080001, partnership on “Telecommunications of the Future” (PE00000001 - program “RESTART”). This work was also supported by Japan Science and Technology Agency (JST) as part of Adopting Sustainable Partnerships for Innovative Research Ecosystem (ASPIRE), Grant Number JPMJAP2517.

REFERENCES

[1] T. Higuchi, M. Takahashi, K. Sasaki, Y. Taguchi, and K. Sanda, “Can vehicles foresee communication disruptions?: Feasibility of v2x network digital twin,” in *2025 IEEE International Conference on Pervasive Computing and Communications Workshops and other Affiliated Events (PerCom Workshops)*, 2025, pp. 633–636.

[2] L. Hui, M. Wang, L. Zhang, L. Lu, and Y. Cui, “Digital twin for networking: A data-driven performance modeling perspective,” *IEEE Network*, vol. 37, no. 3, pp. 202–209, 2023.

[3] Y. Wu, K. Zhang, and Y. Zhang, “Digital twin networks: A survey,” *IEEE Internet of Things Journal*, vol. 8, no. 18, pp. 13 789–13 804, 2021.

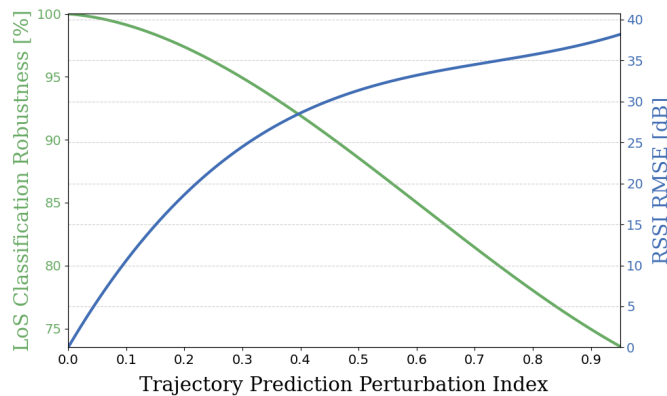


Fig. 5: Experimental RSSI RMSE (blue) and LoS Prediction Accuracy (green) trends for different trajectory prediction perturbation.

[4] K. Wang, Z. Li, K. Nonomura, T. Yu, K. Sakaguchi, O. Hashash, and W. Saad, “Smart mobility digital twin based automated vehicle navigation system: A proof of concept,” *IEEE Transactions on Intelligent Vehicles*, vol. 9, no. 3, pp. 4348–4361, 2024.

[5] R. Pegurri, D. Gasco, F. Linsalata, M. Rapelli, E. Moro, F. Raviglione, and C. Casetti, “Van3twin: the multi-technology v2x digital twin with ray-tracing in the loop,” 2025. [Online]. Available: <https://arxiv.org/abs/2505.14184>

[6] F. Raviglione, C. R. Carletti, M. Malinverno, C. Casetti, and C. Chiasserini, “ms-van3t: An integrated multi-stack framework for virtual validation of V2X communication and services,” *Computer Communications*, vol. 217, pp. 70–86, 2024.

[7] J. Hoydis, S. Cammerer, F. Ait Aoudia, A. Vem, N. Binder, G. Marcus, and A. Keller, “Sionna: An Open-Source Library for Next-Generation Physical Layer Research,” *arXiv preprint*, Mar. 2022.

[8] S. Roongpraiwan, Z. Li, T. Yu, and K. Sakaguchi, “Digital twin-enabled blockage-aware dynamic mmwave multi-hop v2x communication,” 2025. [Online]. Available: <https://arxiv.org/abs/2503.03590>

[9] L. Cazzella, F. Linsalata, M. Magarini, M. Matteucci, and U. Spagnolini, “A multi-modal simulation framework to enable digital twin-based v2x communications in dynamic environments,” in *2024 IEEE 100th Vehicular Technology Conference (VTC2024-Fall)*, 2024, pp. 1–6.

[10] R. Rusca, F. Raviglione, C. Casetti, P. Giaccone, and F. Restuccia, “Mobile RF Scenario Design for Massive-Scale Wireless Channel Emulators,” in *2023 Joint European Conference on Networks and Communications & 6G Summit (EuCNC/6G Summit)*, 2023, pp. 675–680.

[11] T. Gaugel, L. Reichardt, J. Mittag, T. Zwick, and H. Hartenstein, “Accurate simulation of wireless vehicular networks based on ray tracing and physical layer simulation,” in *High Performance Computing in Science and Engineering’11: Transactions of the High Performance Computing Center, Stuttgart (HLRS) 2011*. Springer, 2012, pp. 619–630.

[12] A. Ruz-Nieto, E. Egea-Lopez, J.-M. Molina-Garcia-Pardo, and J. Santa, “A 3D simulation framework with ray-tracing propagation for LoRaWAN communication,” *Internet of Things*, vol. 24, p. 100964, 2023.

[13] M. Zhu, L. Cazzella, F. Linsalata, M. Magarini, M. Matteucci, and U. Spagnolini, “Toward real-time digital twins of em environments: Computational benchmark for ray launching software,” *IEEE Open Journal of the Communications Society*, 2024.

[14] A. Zubow, Y. Pilz, S. Rösler, and F. Dressler, “Ns3 meets Sionna: Using Realistic Channels in Network Simulation,” *arXiv*, cs.NI 2412.20524, 12 2024.

[15] R. Pegurri, F. Linsalata, E. Moro, J. Hoydis, and U. Spagnolini, “Toward digital network twins: Integrating sionna RT in ns-3 for 6G Multi-RAT networks simulations,” in *IEEE INFOCOM WKSHPS: Digital Twins over NextG Wireless Networks (DTWIN 2025) (INFOCOM DTWIN 2025)*, London, United Kingdom (Great Britain), May 2025, p. 5.88.

[16] G. Twardokus and H. Rahbari, “DT-CoVeSS: Advancing NextG C-V2X Security Evaluation through High-Fidelity Digital Twinning,” in *IEEE INFOCOM WKSHPS: Digital Twins over NextG Wireless Networks (DTWIN 2025) (INFOCOM DTWIN 2025)*, London, United Kingdom (Great Britain), May 2025.

[17] M. Elloumi, G. Kaddoum, M. Zoheb Hassan, and B. Selim, “Digital-twin-empowered interference management for multihop internet of vehicles networks over millimeter wave bands,” *IEEE Internet of Things Journal*, vol. 12, no. 11, pp. 17 807–17 827, 2025.

[18] Z. Wang, X. Liao, X. Zhao, K. Han, P. Tiwari, M. J. Barth, and G. Wu, “A digital twin paradigm: Vehicle-to-cloud based advanced driver assistance systems,” in *2020 IEEE 91st Vehicular Technology Conference (VTC2020-Spring)*, 2020, pp. 1–6.

[19] M. Rapelli, C. Casetti, and G. Gagliardi, “Vehicular traffic simulation in the city of turin from raw data,” *IEEE Transactions on Mobile Computing*, vol. 21, no. 12, pp. 4656–4666, 2022.

[20] M. Rapelli, G. S. Pannu, F. Dressler, and C. Casetti, “Content sharing in pedestrian-based micro clouds,” in *2022 IEEE 95th Vehicular Technology Conference: (VTC2022-Spring)*, 2022, pp. 1–6.

[21] L. Italiano, B. Camajori Tedeschini, M. Brambilla, H. Huang, M. Nicoli, and H. Wymeersch, “A tutorial on 5g positioning,” *IEEE Communications Surveys & Tutorials*, vol. 27, no. 3, pp. 1488–1535, 2025.

[22] ITU-R P.2040-1, “Effects of building materials and structures on radiowave propagation above about 100 MHz,” Jul. 2015.